CHEMISTRY OF MATERIALS

ARTICLE

pubs.acs.org/cm

A Novel Wet Chemistry Approach for the Synthesis of Hybrid 2D Free-Floating Single or Multilayer Nanosheets of MS_2@oleylamine (M═Mo, W)

Claudia Altavilla,*[,†] Maria Sarno,[†,‡] and Paolo Ciambelli[†,‡]

[†]NANO_MATES, Research Centre for Nanomaterials and Nanotechnology, University of Salerno, Via Ponte don Melillo 1, 84084 Fisciano (SA), Italy

[‡]Department of Industrial Engineering, University of Salerno, Via Ponte don Melillo 1, 84084 Fisciano (SA), Italy

ABSTRACT: A new wet chemistry approach, based on low-temperature (360 °C) decomposition in oleylamine of single-source precursors containing both metal and sulfur, is proposed for the production of stable free-standing nanosheets of MoS_2 and WS_2. The one-pot synthesis permits high-quality 2D nanosheet crystals of MoS_2 and WS_2 to be obtained with a modular number of nanolayers for units. The layered materials obtained are covered by a dynamic protective coating of oleylamine that stabilizes the suspension, avoids aggregation and oxidation phenomena, and could be easily functionalized with other molecules or nanosystems to introduce new properties to the hybrid organic−inorganic nanocomposite. The reaction products were characterized by X-ray diffraction (XRD), transmission electron microscopy (TEM), attenuated total reflectance Fourier transform infrared spectroscopy (ART-FTIR), field emission scanning electron microscopy (FESEM), X-ray photoelectron spectroscopy (XPS), thermogravimetric analysis coupled with mass spectrometry (TG-MS), and dynamic light scattering (DLS) for particle size distribution (PSD).

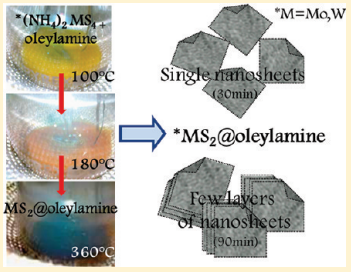

KEYWORDS: inorganic nanosheets, layered materials, 2D crystals, MoS_2, WS_2

1. INTRODUCTION

Stable 2D nanosheet crystals such as transition metal chalcogenides have been emerging as new appealing materials[1−3] thanks to their unique properties that are useful for several applications including new generation of transistors,[4] photoemitting devices,[5,6] nanostructurated photoelectrochemical solar cells,[7] hydrogen storage,[8] catalysis,[9] lubricants,[10−12] Li-ion batteries, and [13,14] double-layer capacitors.[15]

In this context, the possibility of synthesizing 2D crystals of MoS_2 and WS_2 as stable structures of only a few layers is a real challenge because they are unstable and immediately scroll up into closed structures such as quasi-0D onions (IF-nanoparticles) or 1D tubes.[16]

Different strategies have been recently proposed to synthesize these materials on a stable nanometric scale, such as hydrothermal processes,[17] mechanical activation at high temperature,[18] or shape transformation from 1D WS_2 nanorods to 2D nanosheet crystals.[19]

Parallel with traditional intercalation−exfoliation methods for the production of MoS_2 and WS_2 sheets,[1,2] liquid exfoliation in common organic solvent of bulk chalcogenides[20] and scotch tape-based micromechanical exfoliation of natural molybdenite crystals were also recently proposed.[4]

Moreover in the past few years, hybrid organic−inorganic tungstate/molybdate precursors have been proposed as lubricant additives for different oils in several patent applications. The idea was based on the tribochemical formation in situ of layered MoS_2 and WS_2 in the presence of sulfur sources.[21,22]

Herein, a new wet chemistry approach for the production of stable free-standing nanosheets of MoS_2 and WS_2 is described. The innovative synthesis is based on low-temperature (360 °C) decomposition in oleylamine of single-source precursors containing both metal and sulfur.[23] In panel (a) of Figure 1 schematic representation of the synthesis apparatus is shown: it has been used to produce free-standing nanosheets of chalcogenides either as single sheets (30 min reaction time) or assembled with a few multiple sheets (90 min reaction time). Figure 1 also includes some pictures acquired during the synthesis of WS_2@oleylamine nanosheets. It is possible to follow the thermal decomposition of the precursor through the color changes of the reaction mixture. The synthesis product, obtained after a very short time (30−90 min) under nitrogen atmosphere and mechanical stirring, is a stable black oily suspension that can easily turn into a oily paste by centrifugation and/or is dispersed and diluted in several nonpolar solvents, oils, and greases for different applications. The so-obtained nanosheets are made of one or a few layers of crystalline metal chalcogenide covered by an oleylamine organic coating. Thus, the suspension is stabilized, and both aggregation and oxidation phenomena are avoided. Potentially, the coating can be easily functionalized with other molecules or nanosystems to give new properties to such organic−inorganic hybrid nanocomposites. It must be pointed out that because we have found that the number of assembled layers is correlated to the reaction time, and it could be easily controlled.

Received: March 23, 2011
Revised: July 18, 2011
Published: August 11, 2011

2. EXPERIMENTAL SECTION

2.1. Materials. Oleylamine (>70%), ammonium tetrathiotungstate (≥99.9% trace metals basis), ammonium tetrathiomolybdate (99.97% trace metals basis), ethanol, and toluene were purchased from Aldrich and were used as received.

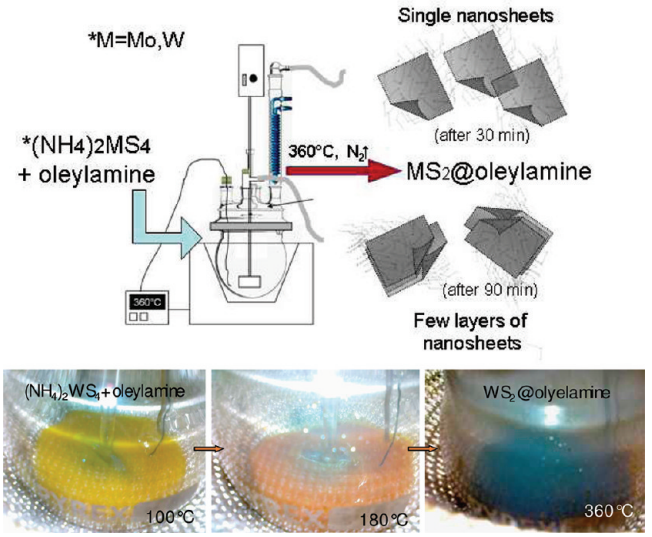

Figure 1. Scheme of the apparatus for the synthesis of 2D MS_2@oleylamine nanosheets by thermal decomposition of thio-salts of Mo and W in the presence of oleylamine. Varying the reaction time, free-standing monolayers or a few assembled layers were obtained. Color changes of the reaction mixture during the synthesis of WS_2@oleylamine suggest that the decomposition of the precursor occurred. In the case of the molybdenum precursor, the color changes from red to black.

2.1. Synthesis of 2D MoS_2@oleylamine Nanosheet Crystals. A total of 2 mmol of $(NH_4)_2MoS_4$ was stirred in 80 mL oleylamine under a N_2 flow at 100 °C for 15 min. The temperature was increased and kept constant at 360 °C for 30 min or 90 min.. The reactor was cooled to room temperature, and a black product was collected.

2.2. Synthesis of 2D WS_2@oleylamine Nanosheet Crystals. A total of 2 mmol of $(NH_4)_2WS_4$ was stirred under a N_2 atmosphere in 80 mL of oleylamine for 15 min at 100 °C. The temperature was increased and kept constant at 360 °C for 30 min or 90 min. The reactor was cooled to room temperature, and the product was collected. To remove the excess surfactant, the samples were repeatedly washed with ethanol and centrifuged.

2.3. Characterization Techniques. TEM micrographs were obtained with a JEOL JEM 2010 electron microscope operating at 200 keV. XPS measurements were carried out using a PE-PHI/SAM-5600 monochromator system spectrometer. XRD patterns (Cu Kα radiation) were collected with a Bruker D8 diffractometer. Field emission scanning electron microscopy images were collected with a FESEM LEO 1550 VP microscope. The nanoparticles were characterized using (ATR) FT-IR. The infrared spectra were acquiered by a Thermo Nicolet attenuated total reflection (ATR) FT-IR spectrometer equipped with a ZnSe crystal cell. The thermal decomposition behavior of the nanosheet organic coating was investigated with a TG-DTG-DSC symultaneous thermo-analyzer (Q600, TA Instruments) online connected to a quadrupole mass detector (Quadstar 422, Pfeiffer Vacuum). Particle size distribution of nanosheet dispersion was determined using a dynamic light scattering (DLS) instrument (HPPS ET− Malvern Instruments).

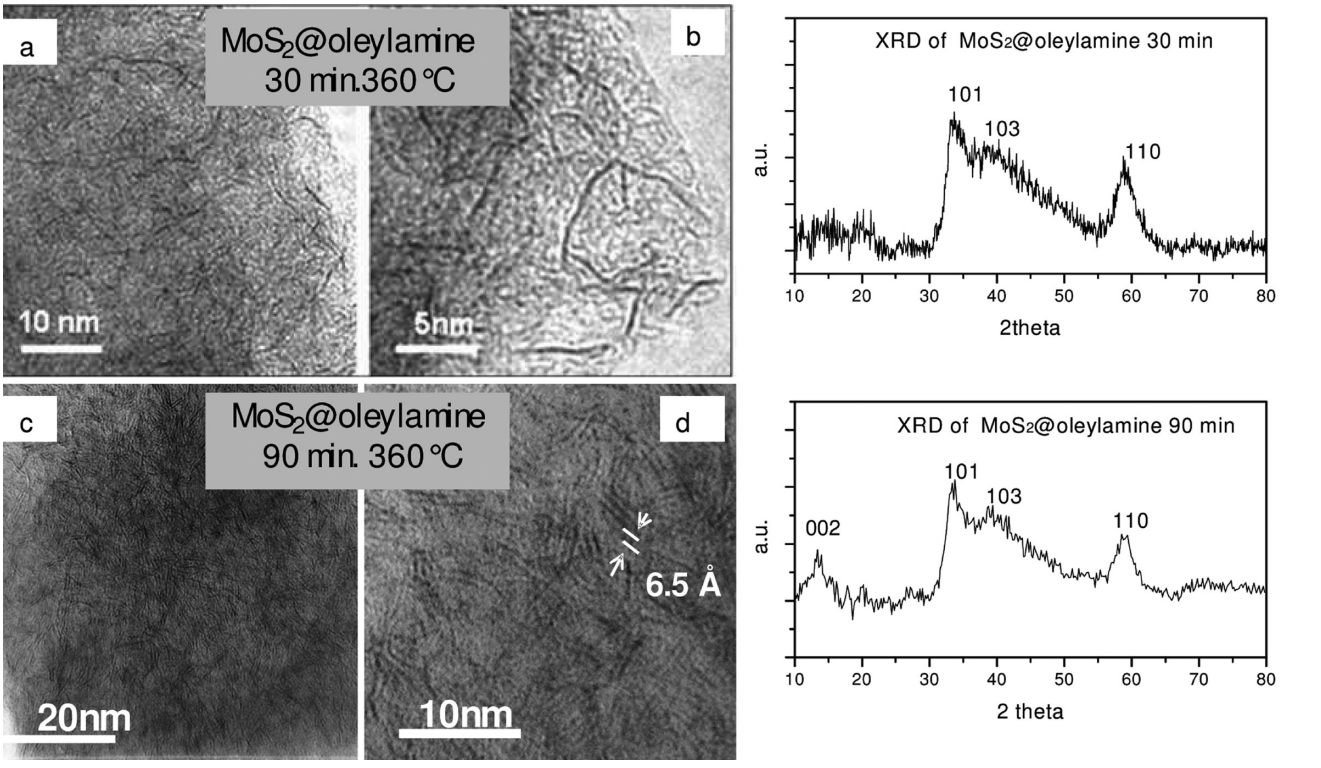

Figure 2. (a) TEM image of MoS_2@oleylamine (30 min at 360 °C); (b) magnified detail of free-standing single nanosheets obtained; (c) TEM image of free-standing multilayer MoS_2@oleylamine nanosheets (90 min at 360 °C); (d) magnified detail of (002) family lattice planes with d = 6.5 Å; on the right side (up) XRD of MoS_2@oleylamine single sheets, and (down) XRD of MoS_2@oleylamine few assembled nanosheets. See the very low intensity of the c axis peak. (ICDD reference card 17−0744).

dx.doi.org/10.1021/cm200837g |Chem. Mater. 2011, 23, 3879–3885

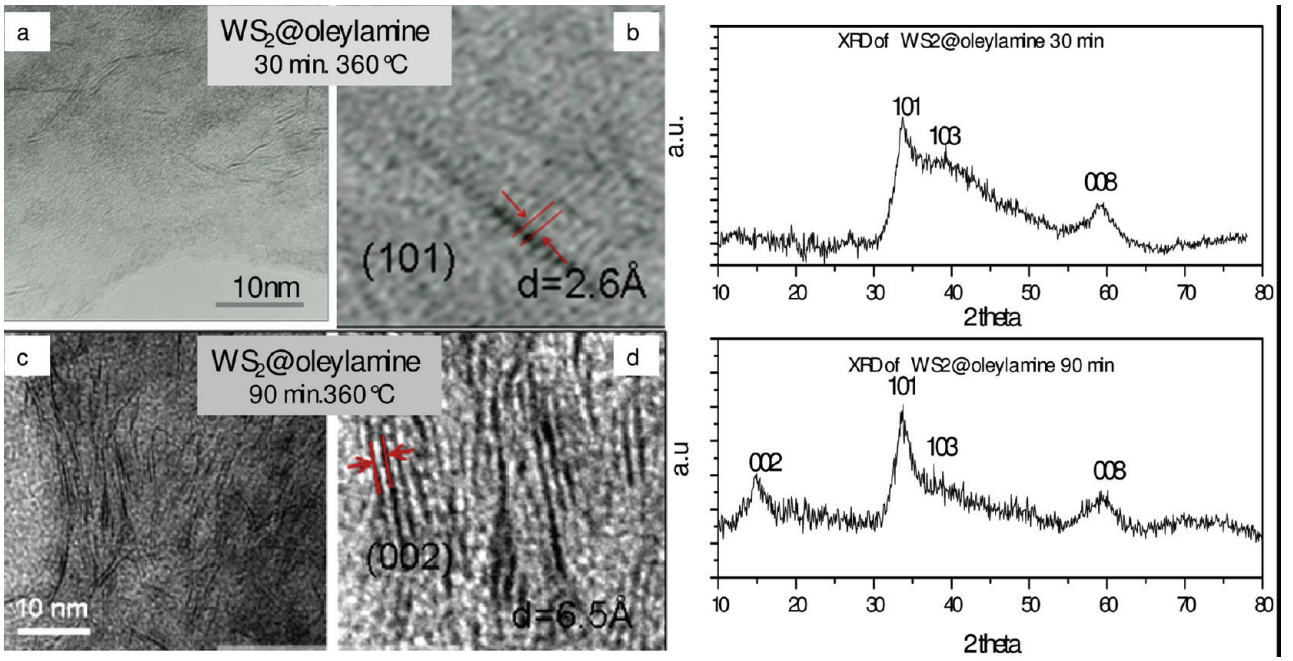

Figure 3. (a) TEM image of free-standing single nanosheets of WS_2@oleylamine (30 min at 360 °C); (b) magnified detail of single sheets, see (101) lattice planes with d = 2.6 Å; (c) TEM image of free-standing multilayer WS_2@oleylamine nanosheets (90 min at 360 °C); (d) magnified detail for d space of (002) family lattice planes with d = 6.5 Å; on the right side (up) XRD WS_2@oleylamine single sheets, and (down) XRD of WS_2@oleylamine few assembled nanosheets. See the very low intensity of the c axis peak. (ICDD reference card 08−0237).

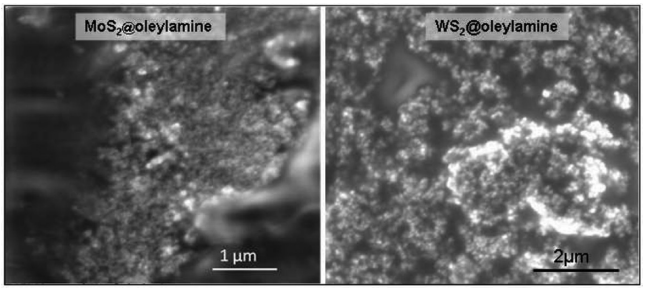

Figure 4. FE-SEM images of MoS_2@oleylamine and WS_2@oleylamine after washing.

3. RESULTS AND DISCUSSION

The reaction products were characterized by X-ray diffraction (XRD), transmission electron microscopy (TEM), field emission scanning electron microscopy (FESEM), X-ray photoelectron spectroscopy (XPS), attenuated total reflection FT- infrared spectroscopy (ATR) FT-IR, thermogravimetric analysis coupled with mass spectrometry (TG-MS), and dynamic light scattering (DLS) for particle size distribution (PSD).

Typical XRD patterns of samples obtained at 360 °C with different reaction times (30 and 90 min), starting from molybdenum or tungsten thiosulphate as precursors, are respectively reported in Figures 2 and 3 (right sides). For the two different reaction times, it is possible to assign the reflection peaks of the family lattices planes (101), (103), (110) for MoS_2 @oleylamine systems (Figure 2) and the reflection peaks of the family lattices planes (101), (103), (008) for WS_2@oleylamine.

For both systems, a peak with a very low intensity, corresponding to (002) reflection of the c axis (d = 6.8 Å) was observed only in the XRD patterns of samples obtained after 90 min of reaction. The (002) peak was completely absent in the XRD of samples obtained after only 30 min of reaction. These results strongly suggest the predominant formation of single layer-MS_2@oleylamine[1,2,9] after 30 min and of materials constituted by a few layers of units assembled by van der Waals interactions after 90 min of reaction.[1,2]

The TEM images confirm the result of XRD analysis and the hypothesis of a reaction time depending on the formation of single or multilayer nanosheets. In Figures 2 and 3, TEM images of MoS_2@oleylamine and WS2@oleylamine obtained after different reaction times are reported. In panels (a) and (b) of Figure 2, single nanosheets of MoS_2@oleylamine (30 min reaction time) are clearly visible, while in the case of MoS_2@oleylamine (90 min reaction time), assemblies of a few layers are observed (Figure 2c,d). They have d space (002) of 6.5 Å ± 1, in good agreement with the value of 6.8 Å given by XRD analysis.

The same behavior was observed in the case of WS_2@oleylamine. In panel (a) of Figure 3, typical TEM images of WS_2@ oleylamine (30 min at 360 °C) free-standing nanosheets are reported. The absence of the assembled sheet unit is clearly visible; moreover in the magnified detail (Figure 3b), the (101) family lattice planes with d = 2.6 Å are visible. On the other hand, after 90 min of reaction, the TEM images acquired on the WS_2@ oleylamine sample show free-standing multilayer nanosheets (Figure 3c,d), and in the magnified detail, there is evidence of the presence of (002) family lattice planes with d = 6.5 Å.

FE-SEM images of MoS_2@oleylamine (30 min) and WS_2@ oleylamine (90 min) samples acquired after the washing treatment are reported in Figure 4. The morphology of both samples is consistent with the presence of little aggregates of average size around 100 nm.

The hydrodynamic diameters of nanosheets in solution were determined by DLS. The DLS technique measures Brownian

dx.doi.org/10.1021/cm200837g |Chem. Mater. 2011, 23, 3879–3885

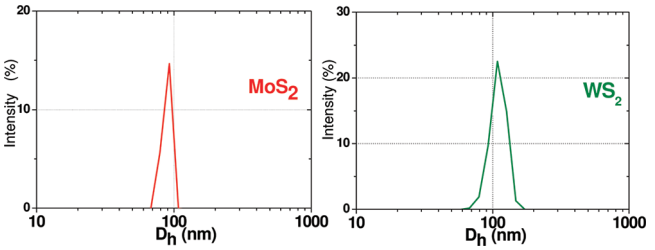

Figure 5. PSD of MoS_2@oleylamine (30 min) and WS_2@oleylamine (90 min) nanosheets as determined by DLS technique.

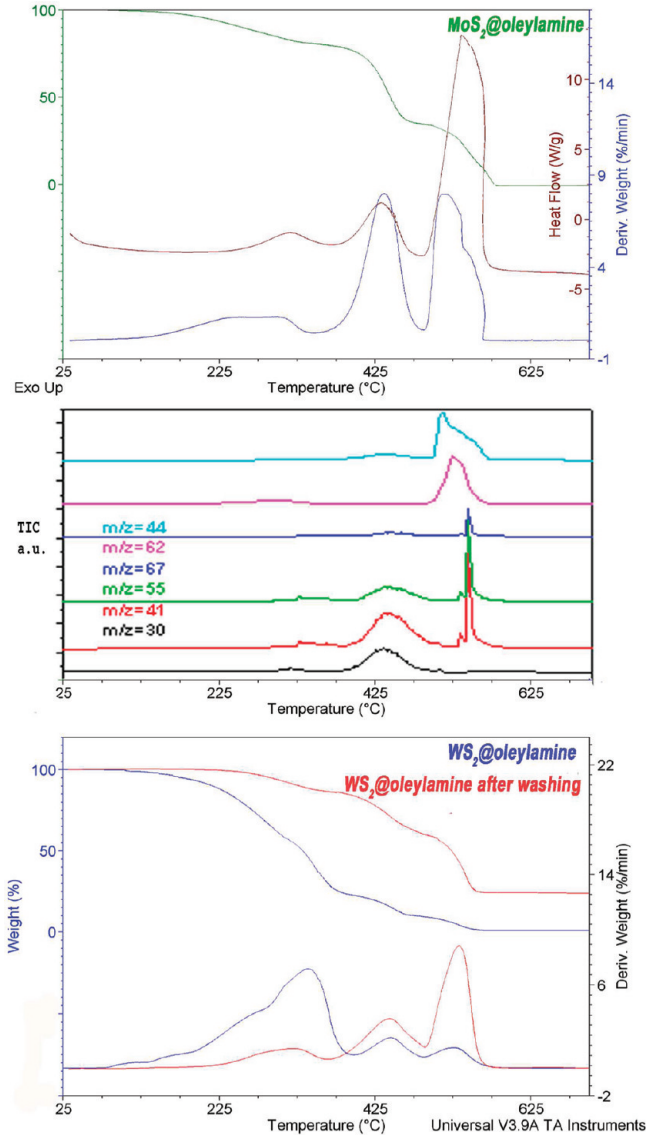

Figure 6. (a) TG-DTG-DSC of MoS_2@oleylamine nanosheets and (b) relevant total ion current signals; (c) TG-DTG of WS_2@oleylamine samples before and after washing.

motion (the random movement of particles due to the bombardment by the solvent molecules that surround them) and relates this to the size of the particles. The size of a particle is calculated from the translational diffusion coefficient by using the

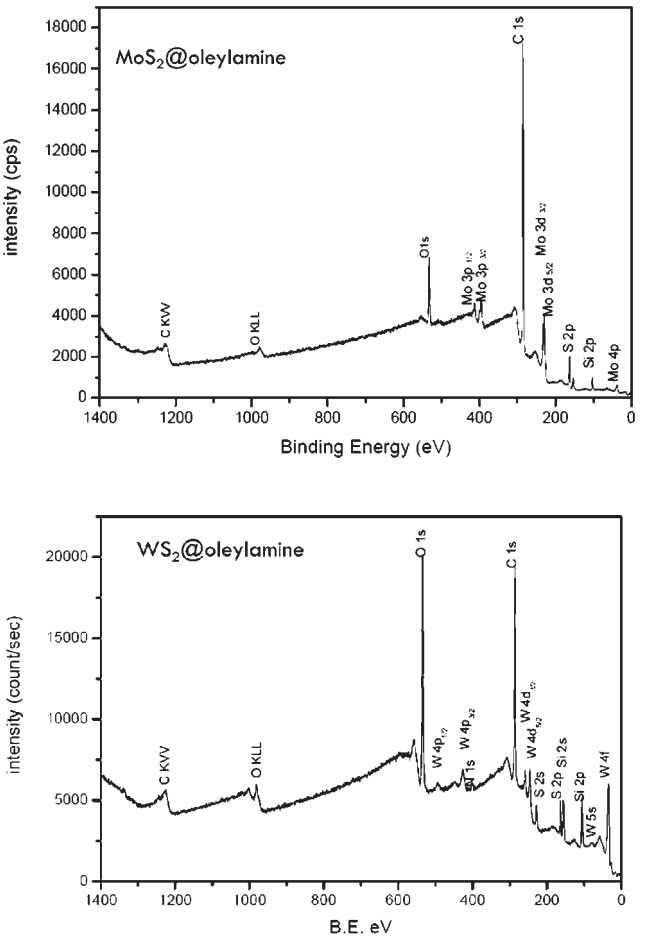

Figure 7. XPS wide spectra of MoS_2@oleylamine and WS_2@oleylamine systems. For both samples, only signals arising from metal chalcogenides and oleylamine coating were detected; no other impurities were observed. The Si signals are due to the support used for the samples.

Stokes−Einstein equation

$$d(\mathrm{H}) = \frac{kT}{3\pi\eta D}$$

where $d(\mathrm{H})$ = hydrodynamic diameter, D = translational diffusion coefficient, k = Boltzmann's constant, T = absolute temperature, and η = viscosity.

The diameter that is measured in DLS is a value that refers to how a particle diffuses within a fluid so it is referred to as a hydrodynamic diameter (the diameter of a sphere that has the same translational diffusion coefficient of the particle).

The hydrodynamic diameters of nanosheets in solution,[24−26] as determined by DLS, are in the range of 70−110 nm for MoS_2@oleylamine (30 min) centered at 94 nm and in the of range 70−170 nm centered at 107 nm for the longer time synthesized WS_2@oleylamine (90 min) (Figure 5). These results are consistent with the SEM observation (Figure 4) showing the samples constituted of quasi-spherical suprastructures containing nanosheets (see the TEM images in Figures 2 and 3). For both systems, the size distribution ranges become a little larger and shift to higher average sizes for the 90 min synthesized samples with respect to those of the 30 min ones.

dx.doi.org/10.1021/cm200837g |*Chem. Mater.* 2011, 23, 3879–3885

The thermal conversion of MS_2@oleylamine (M=Mo, W) in air flow occurred in three main weight loss steps (Figure 6a). The first one is due to sulfur impurities, oxidized during the TG measurements in air flow to SO_2 (see the SO_2 profile in the same temperature range of the weight loss). The second one corresponds to the physisorbed oleylamine decomposition starting at 370 °C (as clearly indicated by the corresponding total ion current (TIC) of the most intense mass fragments peaks: m/z = 30, 41, 55, 67; Figure 7b), and the last one (onset at 480 °C) corresponds to the oxidation of the MoS_2@oleylamine system with exothermal (see the DSC profile in Figure 6a) release of SO_2 (m/s = 64) and CO_2 (m/s = 44). The thermal decomposition of the chemisorbed oleylamine, with the onset point at about 530 °C, is visible, too. It is worthwhile that the oleylamine coating has a strong effect on the thermal behavior of MoS_2 as a main result of the interaction with it: the typical starting oxidation temperature of the molybdenum sulphide was upshifted from 360 °C[27,28] to about 475 °C, at which begins the conversion of MoS_2 to MoO_3 and the release of gaseous SO_2 (see Figure 6b), as reported previously.[25] In panel (c) of Figure 6 the typical TG-DTG profiles of raw and washed WS_2@oleylamine are shown. The significant reduction of the intensity of DTG peaks for the washed samples (Figure 6c) is a consequence of the release of sulfur as SO_2 under the first weight loss and of the oleylamine excess removed by washing.

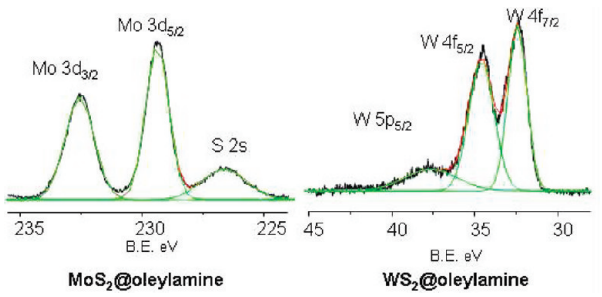

Figure 8. Mo3d XPS spectrum of MoS_2@oleylamine (left) and W4f XPS spectrum of WS_2@oleylamine nanosheets (right).

Table 1. B.E. of Elements in MS_2@oleylamine (M=W, Mo)

MoS_2@oleylamine	$Mo3d_{5/2}$	$Mo3d_{3/2}$	$S2p_{3/2}$	$S2p_{1/2}$
B.E. (eV)	229.3	232.5	162.0	163.1
WS_2@oleylamine	$W4f_{7/2}$	$W4f_{5/2}$ 3	$S2p_{3/2}$	$S2p_{1/2}$
B.E. (eV)	32.4	34.5	162,2	163.2

The B.E. of S2p (Table 1) are consistent with spin orbit $S2p_{3/2}$—$2p_{1/2}$ of S2.[27,28] In the XPS spectrum of the W4f doublet for WS_2@oleylamine (Figure 7, right side), the binding energies of $W4f_{7/2}$ and $W4f_{5/2}$ and $S2p_{3/2}$ (see Table 1) are in good agreement with the values reported for tungsten disulfide.[31−33]

The surface chemistry of Mo and W sulphide was investigated by XPS. For both materials, the wide XPS spectra show only signals arising from metal chalcogenides and oleylamine coating, no other impurities being detected (Figure 7) . The Mo3d XPS spectrum of MoS_2@oleylamine, reported in Figure 8 (left side), shows two strong peaks at 229.3 and 232.5 eV, respectively, attributed to the doublet $Mo3d_{5/2}$ and $Mo3d_{3/2}$. The peak at 226.6 eV can be indexed as S2s. These binding energies (B.E.) correspond to the expected values for MoS_2.[29,30] The presence of other compounds such as Mo_2S_5, MoS_3, or MoO_3, characterized by 3d signals at higher B.E., can be excluded.[27,28]

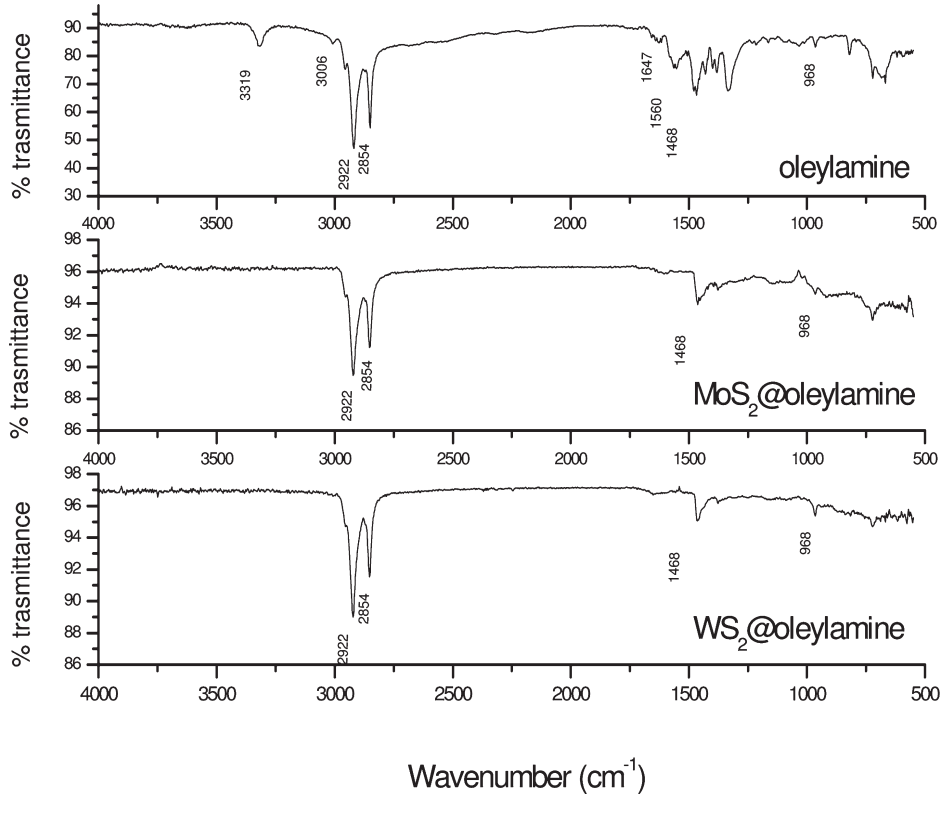

Figure 9. (ATR)FT-IR spectra of pure oleylamine, MoS_2@oleylamine, and WS_2@ oleylamine.

dx.doi.org/10.1021/cm200837g |Chem. Mater. 2011, 23, 3879–3885

No signal of W4f arising from WO_3 species was detected.[34] The S/Mo atomic ratio, as evaluated from XPS spectra, is 2.4 for MoS_2@oleylamine, and the S/W ratio is 2.2 for WS_2@oleylamine. These results could be due to a process of dangling bond passivation at the edges of the nanoplatelets by additional S atoms, as reported in the literature for analogous systems.[35] The higher value of the S/M ratio found for MoS_2 (30 min) with respect to that of WS_2 (90 min) is likely due to, in the first case, the presence of free-standing single sheets and to blocks of few sheets in the second case.

To investigate whether the surface of the nanosheets was capped with oleylamine, the (ATR) FT-IR spectra were acquired. The spectra of pure oleylamine, MoS_2@oleylamine, and WS_2@-oleylamine are reported in Figure 9. The spectrum of oleylamine shows the characteristic peaks of the oleic group in the 2850−3000 cm^{-1} region, the ν (C═C) stretch mode at 1647 cm^{-1}, and the peak at 1468 cm^{-1} due to the (C−H) bending mode. In addition, there are characteristic signals of the amine group: the peak at 3319 cm^{-1} due to the ν (N−H) stretching mode of the primary amine, the peak at 1560 cm^{-1} due to the $-NH_2$ scissoring mode, and the peak due to the $-NH_2$ bending mode at 968 cm^{-1}.[36] In the IR spectra of MS_2 nanocrystals, the presence of the oleylamine as a capping agent on the surface is confirmed by the peak characteristics of the oleic group in the 2850−3000 cm^{-1} region, the ν (C═C) stretch mode at 1647 cm^{-1}, and the peak at 1468 cm^{-1} due to the (C−H) bending mode.[37] Although the presence of the amino group is indicated by the $-NH_2$ bending mode at 968 cm^{-1},[38] the signals of the free primary amine group at 3319 cm^{-1} due to the ν (N−H) stretching mode seem to be absent in the spectra of hybrid chalcogenides, while the peak at 1560 cm^{-1} due to the $-NH_2$ scissoring mode is significantly reduced. This phenomenon was observed also for other kinds of nanoparticles successfully capped by oleylamine.[34]

4. CONCLUSION

We have developed a unique, simple, and versatile one-pot synthetic route for the production of high-quality 2D nanosheet crystals of MoS_2 and WS_2 with a modular number of nanolayers for units. The crystals are covered by a protective coating of oleylamine that stabilizes the suspension, avoids aggregation and oxidation phenomena, and could be easily functionalized. Moreover, this novel wet chemistry approach can be easily scaled up for industrial production. Fuctionalization of organic coatings and synthesis of mixed chalcogenides are in progress.

AUTHOR INFORMATION

Corresponding Author
*E-mail: caltavilla@unisa.it.

ACKNOWLEDGMENT

This work was supported by the seventh Framework Program of the European Community within the AddNano Project (The development and scale-up of innovative nanotechnology-based processes into the value chain of the lubricants market), Contract 229284.

The authors acknowledge Prof. E. Ciliberto of the University of Catania for XPS and FESEM characterizations and Dr. A. Albu-Yaron of Weizmann Institute of Science for TEM images and Dr. E. Avallone for ATR-FT IR spectra.

REFERENCES

(1) Rao, C. N. R.; Nag, A *Eur. J. Inorg. Chem.* **2010**, *27*, 4244–4250.
(2) Matte, H. S. S. R.; Gomathi, A.; Manna, A. K.; Late, D.; Datta, R.; Pati, S. K.; Rao, C. N. R. *Angew. Chem., Int. Ed.* **2010**, *122*, 4153–4156.
(3) Lee, C.; Yan, H.; Brus, L. E.; Heinz, T. F.; Hone, J.; Ryu, S. *ACS Nano* **2010**, *4*, 2695–2700.
(4) Radisavljevic, B.; Radenovic, A.; Brivio, J.; Giacometti, V.; Kis, A. *Nat. Nanotechnol.* **2011**, *6*, 147–150.
(5) Aharon, E.; Albo, A.; Kalina, M.; Frey, G. L. *Adv. Funct. Mater.* **2006**, *16*, 980–986.
(6) Splendiani, A.; Sun, L.; Zhang, Y.; Li, T.; Kim, J.; Chim, C.-Y; Galli, G.; Wang, F. *Nano Lett.* **2010**, *10*, 1271–1275.
(7) Thomalla, M.; Tributsch, H *J. Phys. Chem. B* **2006**, *110*, 12167–12171.
(8) A.M. Seayad, D. M. *Adv. Mater.* **2004**, *16*, 765–777.
(9) Hu, K. H.; Hu, X. G.; Xu, Y. F.; Pan, X. Z *React. Kinet., Mech. Catal.* **2010**, *100* (ì), 153–163.
(10) Wu, Z; Wang, D; Wang, Y; Sun, A *Adv. Eng. Mater.* **2010**, *12*, 534–538.
(11) Mosleh, M; Atnafu, N. D.; Belk, J. H.; Nobles, O. M. *Wear* **2009**, *267*, 1220–1225.
(12) Hua, K. H.; Liua, M.; Wanga, Q. J.; Xua, Y. F.; S. Schraubea, b; Hua, X. G. *Tribol. Inter.* **2009**, *42*, 33–39.
(13) Feng, C; Ma, J; Li, H.; Zeng, R.; Guo, Z.; Liu, H. *Mat. Res. Bull.* **2009**, *44*, 1811–1815.
(14) Liang, Y; Feng, R.; Yang, S; Ma, H.; Liang, J.; Chen, J *Adv. Mater.* **2011**, *23*, 640–643.
(15) Soon, J. M; Loh, K. P. *Electrochem. Solid-State Lett.* **2007**, *10*, A250–A254.
(16) Tenne, R.; Seifert, G. *Annu. Rev. Mater. Res.* **2009**, *39*, 387–413.
(17) Peng, Y; Meng, Z; Zhong, C; Lu, J.; Yu, W; Jia, Y.; Qian, Y. *Chem. Lett.* **2001**, *8*, 772–773.
(18) Wua, Z; Wang, D; Zana, X.; Suna, A. *Mater. Lett.* **2010**, *64* (15), 856–858.
(19) Seo, J.; Jun, Y.; Park, S; Nah, H.; Moon, T.; Park, B.; Kim, J.; Kim, Y. G.; Cheon, J. *Angew. Chem., Int. Ed.* **2007**, *119*, 8984–8987.
(20) Coleman, J. N.; Lotya, M; O'Neill, A.; Bergin, S. D.; King, P. J.; Khan, U.; Young, K; Gaucher, A; De, S.; Smith, R. J.; Shvets, I. V.; Arora, S. K.; Stanton, G.; Kim, H.-Y.; Lee, K.; Kim, G. T.; Duesberg, G. S.; Hallam, T.; Boland, J. J.; Wang, J. J.; Donegan, J. F.; Grunlan, J. C.; Moriarty, G.; Shmeliov, A.; Nicholls, R. J.; Perkins, J. M.; Grieveson, E. M.; Theuwissen, K.; McComb, D. W.; Nellist, P. D.; Nicolosi, V. *Science* **2011**, *331* (6017), 568–571.
(21) David Boudreau, D. U.S. Patent Application 20080234154, 2008.
(22) Ravichandran, R. U.S. Patent Application 20090029888, 2009.
(23) Altavilla, C.; Ciambelli, P.; Sarno, M. Italian Patent Application SA2010A000029, 2010.
(24) Ma, J.; Su, W.; Zhang, Y. J.; Hu, T. J.; Liu, H-Y; Li, B.-Y.; Shi, L.-H.; Xu, J.; Mai, Y.-W. *Macromol. Rapid. Commun.* **2003**, *24*, 676–680.
(25) Lambert, T. N.; Chavez, C. A.; Sanchez, B. H.; Lu, P.; Bell, N. S.; Ambrosini, A.; Friedman, T.; Boyle, T. J.; Wheeler, D. R.; Huber, D. L. *J. Phys. Chem. C* **2009**, *113*, 19812–19823.
(26) Wu, Q.; Sjastad, A. O.; Vistad, Ø.B.; Knudsen, K. D.; Roots, J.; Pedersend, J. S.; Norby, P. *J. Mater. Chem.* **2007**, *17*, 965–971.
(27) Wong, K. C.; Lu, X.; Cotter, J.; Eadie, D. T.; Wong, P. C.; Mitchell, K. A. R. *Wear* **2008**, *264*, 526–534.
(28) Farr, J. P. G. *Wear* **1975**, *35*, 1–22.
(29) Wang, H. W.; Skeldon, P; Thompson, G. E.; Wood, G. C. *J. Mater. Sci. Lett.* **1996**, *15*, 494–496.
(30) Wang, H. W.; Skeldon, P; Thompson, G. E. *Surf. Coat. Technol.* **1997**, *91*, 200–207.
(31) Ouerfelli, J.; Srivastava, S. K.; Bernède, J. C.; Belgacem, S. *Vacuum* **2009**, *83*, 308–312.
(32) Martinez, H.; Benayad, A.; Gonbeau, D.; Vinatier, P.; Pecquenard, B.; Levasseur, A. *Appl. Surf. Sci.* **2004**, *236*, 377–386.

(33) Wong, K. C.; Lu, X.; Cotter, J.; Eadie, D. T.; Wong, P. C.; Mitchell, K. A. R. *Wear* **2008**, *264*, 526–534.
(34) Huirache-Acuña, R.; Paraguay-Delgadoc, F.; Albiterd, M. A.; Lara-Romerod, J.; Martínez-Sánchez, R. *Mater. Charact.* **2009**, *60*, 932–937.
(35) Bertram, N.; Cordes, J.; Kim, Y. D.; Ganteför, G.; Gemming, S.; Seifert, G. *Chem. Phys. Lett.* **2006**, *418*, 36–39.
(36) Shukla, N.; Liu, C.; Jones, P. M.; Weller, D. *J. Magn. Magn. Mater.* **2003**, *266*, 178–184.
(37) Li, N.; Zhang, X.; Chen, S; Hou, X.; Liu, Y.; Zhai, X. *Mater. Sci. Eng., B* **2011**, *176*, 688–691.
(38) Salavati-Niasari, M.; Davar, F; Mir, N. *Polyhedron* **2008**, *27*, 3514–3518.